2026 IEEE International Conference on Robotics and Automation (ICRA 2026)
June 1-5, 2026. Vienna, Austria

A Wirelessly Powered Robotic Capsule Chain for Large Volume Gastrointestinal Liquid Sampling

Bella Boyd[1], Kaan Esendag[1], Liu Du[1], Zaneta Koszowska[1], Jialun Liu[1], Shuhei Miyashita[1,2], and Dana D Damian[1,2]

***Abstract*— Liquid sampling from the gastrointestinal (GI) tract offers significant diagnostic advantages. This study presents a novel magnetically actuated Robotic Capsule Chain (RCC) for large volume liquid sample collection within the GI tract. The RCC incorporates a wirelessly powered, on-demand motorized sampling mechanism that eliminates the need for onboard batteries or microcontrollers. The system demonstrated reliable operation at distances up to 60 mm from the transmitter coil. Validation experiments confirmed effective sealing of the sampling chamber and successful collection of up to 375 µL of fluids with viscosities comparable to those in the GI tract. Navigation and sampling were further demonstrated in a synthetic bowel model. These findings highlight the potential of robotic capsule chains to enable wireless, minimally invasive diagnostic procedures in the GI tract.**

I. Introduction

The human gastrointestinal (GI) tract houses a diverse gut microbiota that plays key roles in nutrient metabolism and immune regulation. Studies show that an individual's microbiota composition can significantly impact both physical and mental health [1], [2]. Further analysis of samples obtained directly from the GI tract can serve as biomarkers for the early diagnosis of diseases such as cancer or diabetes [3], as well as for conditions including small intestinal bacterial overgrowth (SIBO), irritable bowel syndrome (IBS), and celiac disease. Unlike faecal samples, which reflect the overall gut environment [4], local fluid analysis can provide clinically important insights into diseases where regional variation is relevant. It may also support the diagnosis of localized infections. Liquid sampling is one approach to obtain such material. For patients with complex or overlapping symptoms, there may be no single definitive test; in these cases, running multiple complementary analyses on specimen collected from the same location can be particularly valuable. Recent research highlights the importance of applying multi-omics approaches, combining, for example, metagenomics, proteomics, and metabolomics to capture microbial composition, and metabolic outputs together [5]. Each of these analyses requires sufficient material, and dividing a small sample across several workflows is often impractical. Larger volume sampling therefore would offer capability to expand the diagnostic potential, enabling faster diagnosis.

While standard tethered endoscopic procedures can provide localized samples, they are associated with patient discomfort and the risk of gut perforation [6]. Furthermore, conventional endoscopes struggle to reach distal regions of the small intestine [7]. Wireless devices are being explored as an alternative, offering the possibility of swallowing a capsule that travels through the GI tract with minimal discomfort [3], [8]. Several passive sampling capsules have been proposed that rely on chemical coatings to dissolve at the intended sampling region [9]–[12]. For example, in [13], a pH-sensitive enteric coating was used to protect the sampling channels in the stomach but dissolve to enable collection in the small intestine. However, many such designs do not include mechanisms to reseal the sample chamber after collection, leaving material vulnerable to contamination downstream. Another critical limitation is the lack of site-specific, on-demand sampling, where collection and sealing can be triggered only at the desired location. To address this, active mechanisms have been developed that enable controlled triggering and resealing, including magnetic hinges [14], [15], magnetic valves [16], and dehydrated hydrogels that swell after sampling [17]. In [18] mucosal sampling was demonstrated using a shape memory alloy (SMA) spring mechanism. Similarly, in [19], a capsule with two chambers was designed to sample both luminal fluid and intestinal mucus using magnetic torsional springs intended to brush against the mucosa. Despite these advances, most capsule-based sampling devices have been limited to small fluid vol-

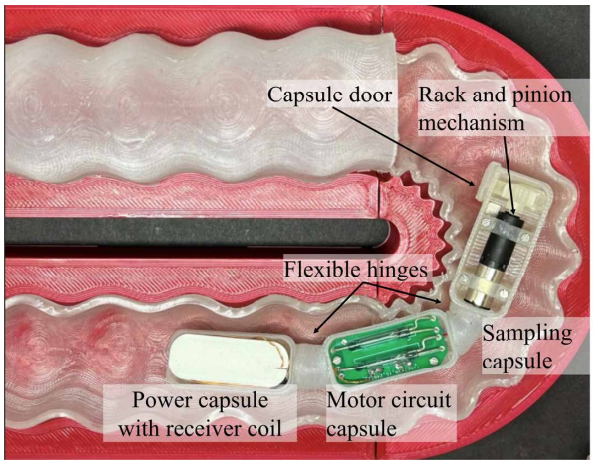

Fig. 1. Cross-sectional view of a wirelessly powered Robotic Capsule Chain (RCC), in a realistically sized silicone bowel model, including a power capsule with receiver coil, control capsule with a motor control circuit and sampling capsule with a pinion and rack mechanism. Capsules are connected with flexible hinges. The capsules are open to show components.

[1]The authors are with the Sheffield Biomedical Robotics Lab, School of Electrical and Electronic Engineering, The University of Sheffield, Sheffield S1 3JD, UK. d.damian@sheffield.ac.uk
[2] Insigneo Institute for *in silico* Medicine, University of Sheffield, UK.

umes, typically in the tens to hundreds of microlitres. While sufficient for a single assay, such volumes are inadequate for multi-test comprehensive analysis. Although recent work has begun to address larger-volume collection [15], there remains a clear need to further maximize liquid sampling capacity in GI tract.

This study presents a novel robotic capsule chain (RCC) designed for large-volume sampling in the GI tract. The RCC can be delivered through a gastroscope and navigated further when required using an on-board magnet. Its sampling mechanism incorporates a DC motor wirelessly powered via an on-board receiver coil, eliminating the need for batteries. The main contributions of this work are: (1) the introduction of a novel concept for a gastroscopically deployed capsule chain enabling on-demand, large-volume sample collection within the GI tract (Fig. 1), with the potential to functionalize multiple capsules in future; (2) a method for wirelessly powering and controlling a DC motor–based sampling mechanism without an on-board battery or microcontroller.

II. Materials & Methods

A. Capsule Assembly Design and Fabrication

The RCC is composed of three capsules, as displayed in Fig. 2. The lead capsule in the assembly, the sample capsule, contains the sampling mechanism and a sample chamber with approximately $400\,\mu$L capacity. Adjoined to this is a capsule containing the RCC's electronics, hereon in referred to as the motor control circuit (MCC). The final capsule in the assembly, the power capsule, contains the RCC's power supply in the form of a wireless power receiver coil.

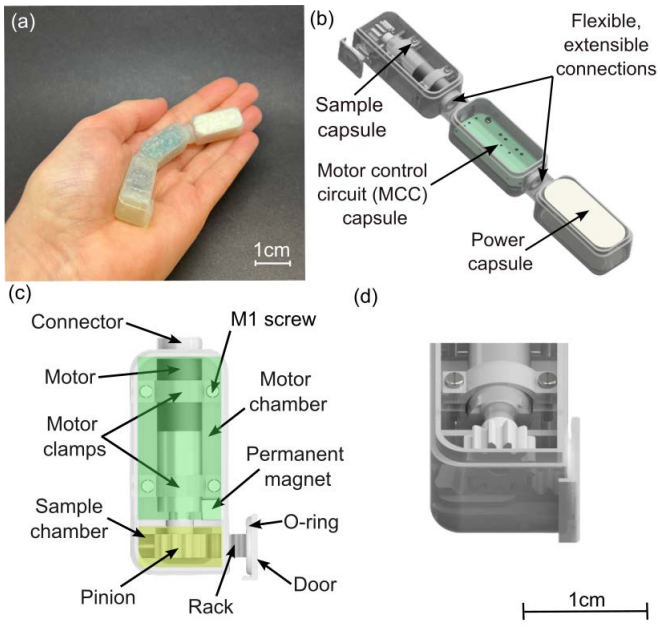

Fig. 2. The three capsule RCC for GI sampling: (a) image of the RCC; (b) CAD render of the RCC without capsule lids to visualize inner components (c) a labelled top view of the sampling capsule's components highlighting the two sub-chambers and the rack and pinion mechanism in the open position (d) a zoomed view of the sampler in the sealed position with scale bar.

Electrical interconnections between capsules are protected with flexible Ecoflex™ 30 (Smooth On Inc.) connectors attached to extrusions on the ends of each capsule. Excluding connectors, the external dimensions of both the MCC and power capsules are $12\times12\times28$ mm and the sample capsule $12\times12\times30$ mm. Fig. 2 (c-d) shows the contents of the sample capsule and its division into two sub-chambers: the sample chamber, which includes a miniature rack and pinion sampling mechanism and space for sample storage; and the motor chamber, which houses a 4-stage planetary gear DC motor (ZWPD006006-700, Generic) of length 21 mm, diameter 6 mm and resistance $18.8\,\Omega$ as well as a 3 mm cubic neodymium permanent magnet for navigation purposes. The rack and pinion sampling mechanism converts the rotary motion of the motor into linear motion for opening and sealing the sample chamber door. In the sealed position, the motor closes the sample chamber by pulling a silicone O-ring gasket on the door tightly against the capsule's exterior surface. The capsule bodies, motor clamps and the sampling mechanism parts (rack, pinion and sample chamber door) were all manufactured with a Form 3 SLA printer using durable resin (Formlabs). Superglue was used to attach the capsule lids to their body counterparts.

B. Motor Control Circuit

The MCC was designed to perform two primary functions: AC to DC rectification and motor direction reversal. A full-bridge rectifier, combined with a smoothing capacitor, converts the AC voltage from the wireless power receiver into the DC voltage required for the motor. Motor reversal is achieved through an H-bridge configuration consisting of two single-pole double-throw reed switches positioned around the motor. When exposed to an external magnetic field, provided by an N52 neodymium permanent magnet (25.5×11 mm), both reed switches actuate simultaneously, reversing the motor by inverting the current direction. The MCC was designed on a two layer PCB of approximate dimension 25.5×11 mm to fit inside the capsule.

C. Wireless Power Transfer (WPT) System

Power is provided to the DC motor in the RCC via a near-field inductively coupled wireless power transfer (WPT) system [20]. Passing alternating current through a transmitter (Tx) coil external to the patient's body creates a time-varying magnetic field which, when coupled with the receiver (Rx) coil in the capsule, induces an alternating electromotive force (EMF) in the Rx. To characterize the operational range and identify the optimal Rx coil, three coil designs were tested across varying Tx–Rx separation distances. The coils were fabricated with single, double and triple stranded 0.2 mm diameter litz wire. Each winding was separately wrapped around a PLA substrate as many times as was required to make three mono-axial coils of identical dimensions matching the capsule size, $9\times10\times24$ mm. The self-inductance and resistance values of each coil were measured using a digital LCR meter (Proster BM4070). The same planar Tx coil, of inductance $19.3\,\mu$H, resistance $0.1\,\Omega$ and inner and outer

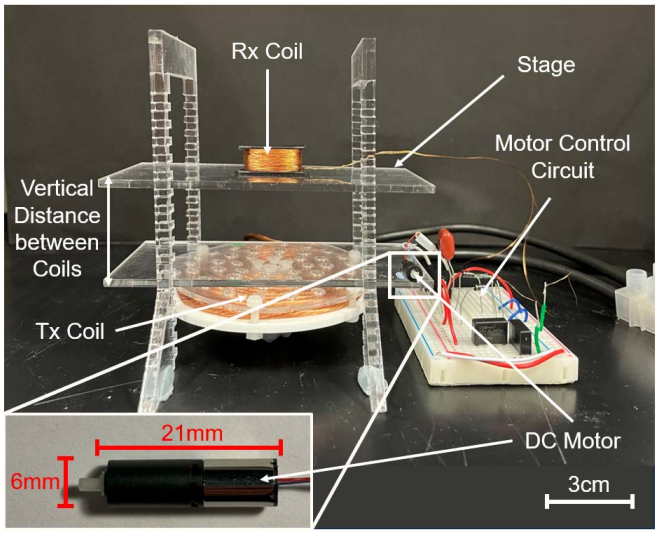

Fig. 3. The experimental setup for characterizing the maximum operating distance between Rx and Tx coils which allowed successful actuation of the motor.

diameter 20 mm and 70 mm respectively, was used to test the WPT capability of each Rx coil using the experimental setup displayed in Fig. 3. A Zero Voltage Switch (ZVS) circuit was used to produce alternating current of peak magnitude 10A through the Tx coil at a frequency, f_0, of 54 kHz. Each Rx coil in turn was connected to the MCC along with the DC motor. Power transfer between Rx and Tx circuits was maximised each time by ensuring resonant conditions via appropriate selection of capacitors to compensate for the differing inductive reactances at each Rx coil at f_0. The Rx coils were placed axially above the Tx on an acrylic stage and the distance between their vertical centres incrementally reduced. At each distance the peak AC voltage induced in the Rx coil, V_{pk}, and the average DC voltage across the motor, V_{motor}, were measured with an oscilloscope (TDS210, Tektronix) and the spinning status of the motor was noted. This process was repeated three times for each coil. The mean and standard deviation of V_{pk} and V_{motor} measurements were calculated across the three trials for each Rx. Inverse square models of the form,

$$V_{pk} = \frac{\theta}{D^2}, \tag{1}$$

were fitted to the experimental data for the mean V_{pk} at each distance using ordinary least squares regression, where D is the vertical distance between Rx and Tx coils and θ is the modelled parameter relating to their mutual inductance.

D. Sampler Force

Measuring the force generated by the rack-and-pinion mechanism is essential to evaluate whether the wireless power transmission can adequately drive the DC motor in a clinically relevant way. Clinically, the capsule may encounter peristaltic pressures and frictional resistance depending on its orientation in the GI tract, both of which must be overcome to open the sampling chamber. Therefore, the rack-and-pinion mechanism must produce forces greater than these physiological loads, previously reported as approximately 0.5 N [21]. The linear force generated by the RCC's rack and pinion sampling mechanism was estimated by measuring the extensions of a tension spring during DC motor/pinion actuation. One end of the spring was attached to the rack and the other to a stationary point on a force measurement test-bed. The motor was powered with the double stranded Rx coil and MCC (section II-B). Using the same experimental setup as described in section II-C, the distance between WPT Tx and Rx coils was varied. At each distance the maximum spring extension, e, caused by the motion of the rack and pinion mechanism (i.e. the extension at the point when the motor/pinion stopped rotating) was measured. The linear force, F_s, generated by the rack and pinion sampling mechanism at each Rx/Tx separation distance was then calculated as $F_s = ke$, with k either 0.08 N/m or 0.16 N/m depending on the spring used. The lower value of spring constant was used to measure extensions at larger Rx/Tx separations when the forces generated by the sampling mechanism were smaller. Conversely, when Rx/Tx separations were smaller and forces larger, the stiffer spring was used.

E. Sample Chamber Sealing

To evaluate the robustness of the RCC's sample chamber sealing and ensure it remains closed under gastrointestinal transit conditions, the chamber was first filled with liquid and then subjected to agitation on a laboratory shaker to simulate mechanical disturbances (Fig. 4 (a)-(d)). Firstly, a blue fluid was made by adding food coloring to deionized water. A syringe filled with 1 mL of this fluid was then used to fill the sample chamber of the RCC which was then sealed (Fig. 4 (a)). The RCC was placed inside a beaker filled with 25 mL clear deionized water and mounted on a shaker (Cole-Parmer Compact Orbital) to facilitate fluid agitation. (Fig. 4 (b)). The beaker with RCC was then shaken at 80 rpm. After 90 minutes, the capsule assembly was removed from the beaker and vials were filled with samples of the following fluids: (A) deionized water - the fluid initially surrounding the capsule; (B) the fluid surrounding the capsule after 90 minutes of shaking; (C) 25 mL of clear deionized water mixed with 1 mL of the blue sample (i.e. the fluid that would have surrounded the capsule after 90 minutes if all of its contents had leaked out); and (D) the blue capsule filling (Fig. 4 (c)). To check for any traces of blue color in fluid (B), which would indicate leakage from the sample chamber, the absorbance spectra of fluids (B), (C), and (D) across the wavelength interval 300-900 nm were characterized with a spectrophotometer (Jenway Genova Plus) using fluid A as the blank measurement. (Fig. 4 (d)).

F. Sampling Capacity

To evaluate the performance and capacity of the capsule's sampling, test were conducted across fluids of varying viscosities and measured the collected volumes.

Four fluids were selected: water (1 mPa); corn oil (51.6 mPa); sesame oil (60.4 mPa); and olive oil (77.1 mPa) [22]. These were chosen to mimic the viscosity of healthy human digestive mucus - healthy gastric mucus has previously been found to be around 85 mPa with a shear rate of $1.15\,s^{-1}$ [23] - noting that it is a non-newtonian fluid. Each fluid was then sampled, and the volume collected in the sample chamber was measured. A large beaker was filled with approximately 25 ml of each sampling fluid and the RCC was placed in the beaker, such that the sampling capsule was submerged in the fluid. The WPT system was used to trigger the opening of the sample chamber door to allow fluid collection for approximately 1 minute. The chamber was then resealed using the WPT system with the addition of the DC magnetic field provided by a permanent magnet required for motor reversal. The RCC then was removed from the beaker, its outer surface wiped dry and placed in a smaller beaker. The contents of the sample chamber were collected with a syringe and their weight was measured and converted to a volume using the known density of the sample fluid under test. This process was repeated five times for each sampling fluid and the average collection volume was calculated.

G. Sealing Demonstration

This section demonstrates the sealing performance post-sampling. A silicone phantom of the small intestine was divided into two sections: the first section containing oil dyed with red pigments; and the second section containing oil without any dye. Olive oil was selected over other oils due to having the closest viscosity to that of human digestive mucus (77.1 mPa). The capsule was placed in the first section of the phantom and navigated with a handheld permanent magnet along its length. The WPT system was then activated to power the motor and open the sample chamber door.

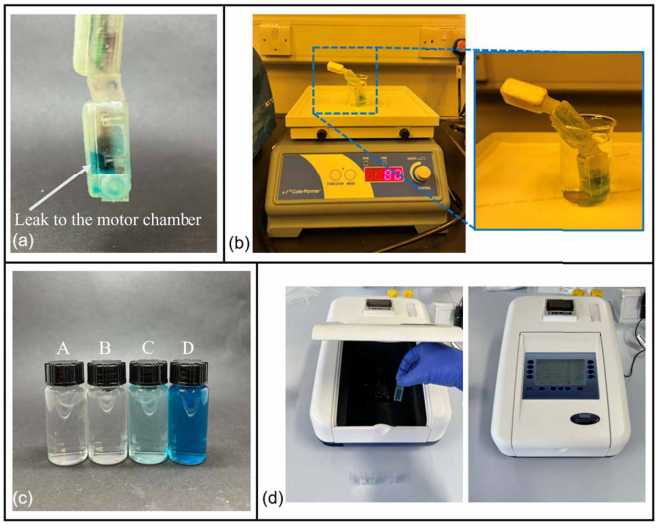

Fig. 4. Stages of the sealing performance experiment: (a) The sampling capsule filled with blue fluid; (b) RCC inside deionized water on top of a shaker; (c) Fluids A-D (from left to right) collected during the experiment; (d) Analyzing the absorbance spectra of the fluids in a spectrophotometer.

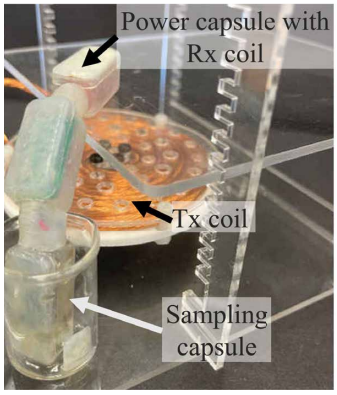

Fig. 5. Sampling performance capacity experiment, showing the power capsule with an embedded Rx, at a distance D from the Tx coil and the sampling capsule submerged in a fluid.

After the sampling chamber was filled, it was sealed by bringing the permanent magnet close to the capsule. The sealed capsule then was manually placed in the non-dyed section of the phantom and navigated along it to verify that no colored fluid leaked, thereby demonstrating effective sealing of the sample chamber.

III. Results

A. Wireless Power Transfer Performance

The experimentally characterized relationship between V_{pk}, and the vertical distance between Tx and Rx coils, D, is displayed in Fig. 6 (a). The data from all three Rx coils show a close adherence to their respective inverse square regression models, which highlights the rapid attenuation of magnetic field strength and coupling between Tx and Rx coils that occurs with distance. V_{pk} also reduces with the number of strands in the Rx coil winding. This is most likely due to the decrease in coil self-inductance which occurred as winding thickness increased, allowing fewer turns to fit within the Rx coil volume (Table I). Despite the single-stranded Rx coil inducing the highest values of V_{pk} across all distances, it was the double stranded Rx which achieved the largest maximum operating distance (MOD) for motor actuation (i.e. the maximum value of D for which the motor was operating) of the three coils, at 62 mm. As Fig. 6 (b) highlights, for coil separation distances greater than 44 mm, the double-stranded coil consistently produces the largest voltage across the motor. It is therefore able to reach/pass the threshold value of V_{motor} which generates sufficient power to actuate the motor at a higher value of D than single-stranded and triple-stranded coils. The MOD is likely smaller in the single-stranded compared to the double-stranded coil due to the higher resistance of the single-stranded winding, highlighted in table I. A higher coil resistance will reduce both the overall power transferred to the Rx circuit and also the fraction of this power usefully transferred to the motor [24]. Despite having the smallest resistance of all three Rx coils, the triple-stranded coil also has the lowest self-inductance which is likely the limiting factor in its MOD.

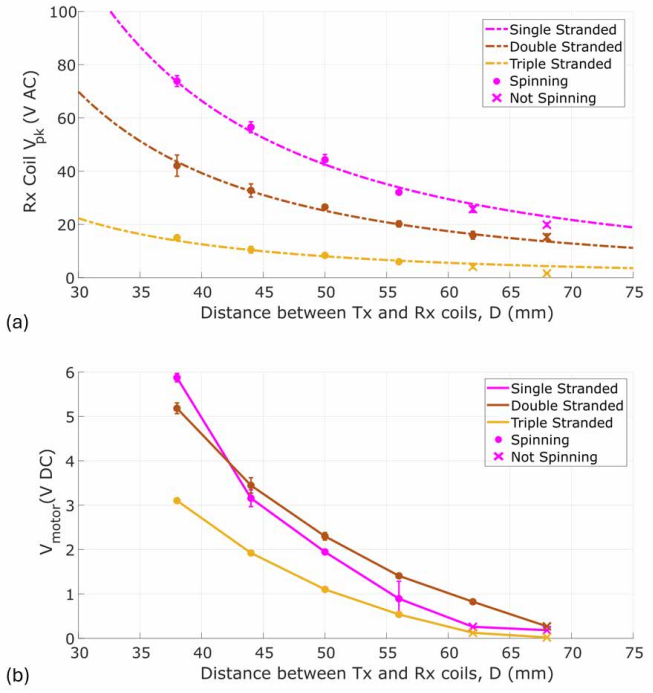

Fig. 6. The motor spinning status and (a) the peak induced voltage in the Rx coil, V_{pk}, and (b) the DC voltage across the motor, V_{motor}, versus the vertical distance between Tx and Rx coils, D, for the single (pink), double (brown) and triple (yellow) stranded Rx coils. Data points are plotted as the mean of three trials with standard deviation error-bars. Dashed lines highlight inverse square models fitted using ordinary least squares and solid lines show linear interpolation between data points.

The double-stranded Rx coil, therefore, achieves the optimal trade-off between Rx coil self-inductance and resistance to maximize motor operating distance. Despite this, during clinical trials, D could vary from 2 cm to more than 10 cm as the Rx coil moves through the GI tract [25], highlighting that even the double-stranded Rx coil would struggle to receive sufficient power to actuate the motor in some regions of the GI tract. Increasing the relative permeability of the Rx coil core material and/or optimizing the characteristics of the Tx coil further are two avenues which could be investigated in future to increase the MOD of the WPT link further.

B. Sampler Force

The linear force characteristic of the sampling mechanism is shown in Fig. 7 and shows that F_s decreases rapidly with distance between WPT coils. The linear force produced by the rack and pinion is just less than 7 N at the smallest separation distance of 32 mm and decreases to 0.4 N by the largest separation distance of 62 mm. In [21], a capsule of comparable diameter to the assembly developed in this work was reported to require an estimated force of 0.5 N to overcome the combined peristaltic and frictional forces in the GI tract. Thus, Fig. 7 suggests that, for coil separation distances less than 60 mm, the rack and pinion mechanism could generate sufficient linear force to reliably open the sample chamber door to obtain a sample. With the sampling mechanism also capable of producing relatively large forces, upwards of 5 N, at small coil separation distances, the safety of the system might be a concern. However, the pressures associated with a 5 N force spread across the surface of the sample chamber door, approximately 90 mm^2, are in the region 0.06 N/mm^2, and much lower than the magnitudes associated with damaging or puncturing tissue [26].

TABLE I

MEASURED SELF-INDUCTANCE AND RESISTANCE VALUES OF THE SINGLE-STRANDED, DOUBLE-STRANDED AND TRIPLE-STRANDED RECEIVER COILS.

Number of Strands in Winding	Inductance (mH)	Resistance (Ω)
1	1.4	11.7
2	0.64	8.2
3	0.24	2.6

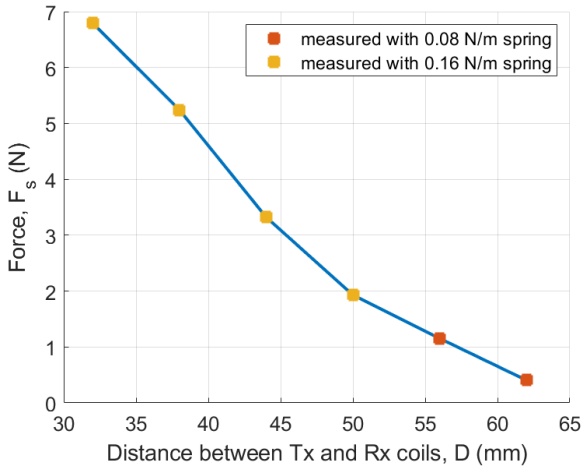

Fig. 7. The linear force produced by the rack and pinion sampling mechanism, F_s, versus separation distance between Rx and Tx coils, D.

C. Sample Chamber Sealing

The absorbance spectra of the fluids B, C and D obtained from the sealing experiment are presented in Fig. 8. The fluid surrounding the capsule assembly after 90 minutes in the silicone intestine model, B, does not appear to contain any traces of blue, with its spectrum remaining at or close to zero for the entire wavelength range tested, highlighting its similarity to the blank measurement, fluid A. Fluid B does not contain a spectral peak in the region 620-635 nm which is a defining feature of the spectra of both blue fluids C and D. This suggests that the O-ring gasket formed an effective seal around the sample chamber and prevented the leakage of substances to and from the chamber. The implications of this are that the RCC could facilitate site-specific sample collection by sealing the sample chamber both prior to and after sample collection has taken place. Fig. 4 (a) does, however, highlight some leakage from the sample chamber into the motor chamber within the RCC sample capsule itself, which allowed it to be filled with 1 mL of fluid as opposed to 400 μL in line with the chamber capacity.

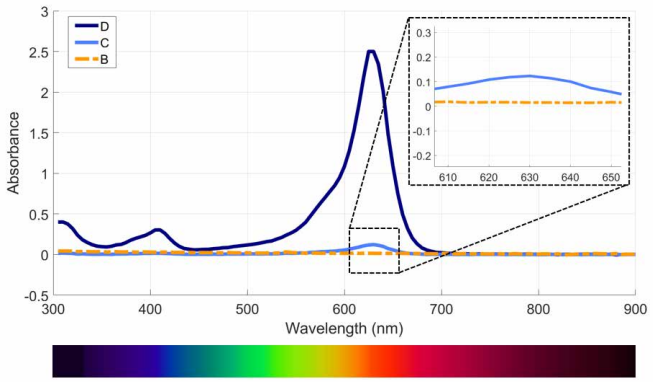

Fig. 8. The absorbance spectra of fluids (B), (C), (D) obtained from the sealing experiment. Fluid (B) was the fluid surrounding the capsule after 90 minutes of shaking. Fluid (C) is the fluid that would have surrounded the capsule after 90 minutes if all of its contents had leaked out (25 mL of clear deionized water mixed with 1 mL of fluid (D)). Fluid (D) was the blue fluid used to fill the capsule sample chamber. Fluid (A) - clear deionized water - was used as the spectrophotometer blank.

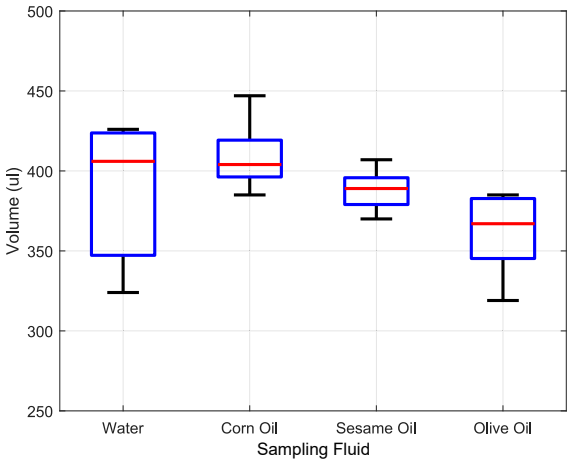

Fig. 9. Capsule collection from 4 different fluids. The viscosity of the liquids are listed in ascending order from left to right with water (1 mPa); corn oil (51.6 mPa); sesame oil (60.4 mPa); and olive oil (77.1 mPa) [22].

D. Sampling Performance

The outcome of the sampling capacity experiments are given in Fig. 9 and show that across all four fluids, the average sampled volume which was collected from the RCC sample chamber was between 350 μL to just over 400 μL. A trend emerges that the higher the fluid viscosity, the lower the volume of fluid successfully sampled and collected. The average sampled volume collected for water was approximately 400 μL, as expected, but there was a much larger deviation across the five trials than the rest of the fluids. This could potentially be attributed to the higher surface tension of water compared to the oils (72 mN/m for water and 32 mN/m for olive oil), which might make it more difficult for the water to enter the sample chamber.

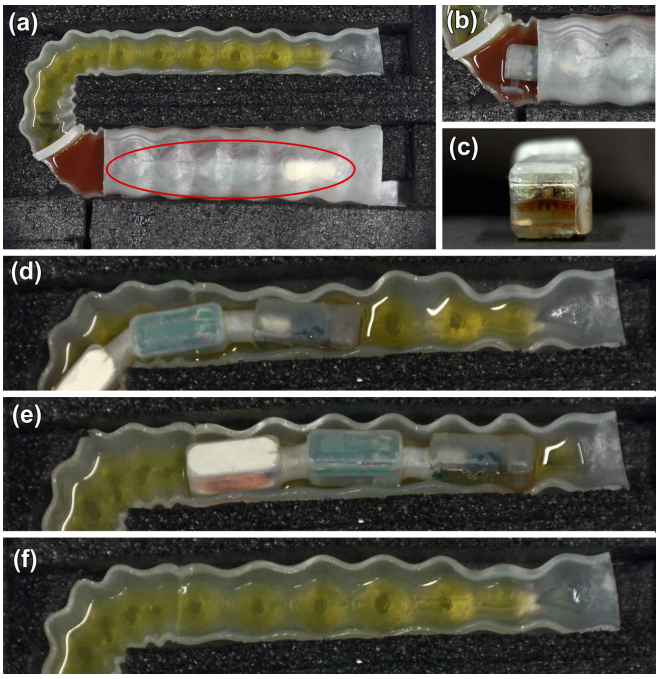

Fig. 10. Demonstration of navigation, operation and successful sealing of collected fluid. (a) The capsule is placed in an intestine phantom, one section covered with olive oil with red dye and the other section without dye. (b) The capsule is navigated to the target location and the sampling mechanism is used to collect the sample. (c) Front view of the capsule showing the collected sample of olive oil with red dye. (d-f) The capsule is placed back into the region with olive oil without red dye and navigated through. There was no trace of red dye after the capsule was removed.

E. Navigation Trial

Fig. 10 shows the overall process of the RCC navigation, sampling and sealing in one experiment. Fig. 10 (a-b) shows the RCC navigated to the target sampling section within red dyed olive oil, where sampling is triggered and the sample chamber subsequently sealed. Fig. 10 (c) shows the sampled fluid as a result. Then the capsule was placed and navigated in the non-targeted section containing non-dyed oil (Fig. 10 (d-e)). The RCC was then removed and Fig. 10 (f) shows that none of the red olive oil leaked into the non-dyed section during the navigation. This demonstrates the non-targeted section was not contaminated, showing the sample chamber sealing efficacy within the RCC.

IV. Discussions & Conclusions

This paper presents a three-chamber RCC designed for active, on-demand large-volume liquid sampling in the GI tract. The study led to the development and testing of a wireless power system for the capsule chain, which demonstrated effective operation at a distance of up to 62 mm. Additionally, a circuit for dual-direction motor control was created without the use of a microcontroller. The capsule's functionality was validated through tests of its sampling capability, including assessments of sampler force, sample chamber sealing performance, and sampling efficacy, with the capsule successfully retrieving approximately 375 μL of olive oil. The capsule chain can be introduced into the GI

tract via endoscopic methods. Once introduced in the upper GI tract, it can be magnetically navigated further and positioned for sampling. In the current RCC design, one capsule is functional while the other two supply power, housing the receiving coil and motor control circuit. Future efforts will focus on redesigning the system so that a greater proportion of the RCC is functional, potentially incorporating additional endoscopic capabilities such as a camera or sensing. These functions, along with dedicated localization modules (e.g., magnetic tracking [27] or RF-based telemetry), will be essential for accurately obtaining the real-time position of the capsule chain within the gastrointestinal environment, thereby enabling precise, site-specific sampling.

A limitation of the current validation is the use of a simplified silicone phantom and bench-top shaker, which do not fully replicate the dynamic conditions of the human GI tract. This initial study focused on baseline mechanical and wireless functional validation. Future in-vitro experiments will evaluate the performance of RCC in anatomically realistic gut simulators that incorporate dynamic fluid flow, physiological temperatures, pH-controlled environments, and simulated peristaltic motion. As for the validation of WPT, while the current study successfully validates the functional actuation of the motor at distances up to $62\,\mathrm{mm}$, the overall WPT efficiency and specific thermal behavior require further quantitative characterization. Given that the active sampling mechanism operates for a very short duration, significant thermal accumulation is highly unlikely. However, continuous operation testing and direct measurement of the capsule surface temperature will be conducted in future work to strictly ensure compliance with the $< 41^{\circ}\mathrm{C}$ thermal safety threshold for in-vivo medical devices.

While this study successfully quantifies the total collected volume as a primary measure of sampling capacity, a more granular analysis of sampling efficiency is required. Future investigations will evaluate the flow-rate dynamics during chamber filling, the influence of varying capsule orientations (which may introduce air bubbles), and edge-case failure modes (e.g., partial obstruction by debris) to ensure high reliability across diverse GI conditions.

For this proof-of-concept prototype, SLA printing resin and silicone elastomers were used. To ensure biocompatibility and long-term material stability in highly acidic and enzymatic digestive conditions, future iterations of the RCC will adopt medical-grade, FDA-approved materials, such as biocompatible SLA resins or injection-molded PEEK. These materials will undergo rigorous short-term soak tests and cytotoxicity evaluations prior to clinical translation.

Further work will also target increasing the maximum operating distance of the wireless power transfer, testing the capsule in in-vivo environments, and advancing miniaturization of the device. Strategies will include combining the MCC and power receiving coil onto a single PCB within the motor chamber, customizing the motor dimensions, and reducing the total number of capsules to create a more compact, unified structure. In parallel, alternative assembly and disassembly strategies of the capsules will be investigated, with the aim of developing a fully non-invasive and modular platform suitable for ingestion rather than endoscopic deployment.

REFERENCES

[1] Y. Fan and O. Pedersen, "Gut microbiota in human metabolic health and disease," *Nature Reviews Microbiology*, vol. 19, no. 1, pp. 55–71, Jan 2021.

[2] A. M. Taylor, S. V. Thompson, C. G. Edwards, S. M. A. Musaad, N. A. Khan, and H. D. Holscher, "Associations among diet, the gastrointestinal microbiota, and negative emotional states in adults," *Nutr Neurosci*, vol. 23, no. 12, pp. 983–992, Feb. 2019.

[3] M. Rehan, I. Al-Bahadly, D. G. Thomas, W. Young, L. K. Cheng, and E. Avci, "Smart capsules for sensing and sampling the gut: status, challenges and prospects," *Gut*, vol. 73, no. 1, pp. 186–202, 2024.

[4] W. Yan, C. Sun, J. Zheng, C. Wen, C. Ji, D. Zhang, Y. Chen, Z. Hou, and N. Yang, "Efficacy of fecal sampling as a gut proxy in the study of chicken gut microbiota," *Front Microbiol*, vol. 10, p. 2126, Sep. 2019.

[5] M. Rios-Morales, M. P. van Trijp, C. Rösch, R. An, T. Boer, A. Gerding, N. de Ruiter, M. Koehorst, M. R. Heiner-Fokkema, H. A. Schols, D. J. Reijngoud, G. J. Hooiveld, and B. M. Bakker, "A toolbox for the comprehensive analysis of small volume human intestinal samples that can be used with gastrointestinal sampling capsules," *Scientific Reports*, vol. 11, no. 1, pp. 1–14, 2021.

[6] I. Levy and I. M. Gralnek, "Complications of diagnostic colonoscopy, upper endoscopy, and enteroscopy," *Best Pract Res Clin Gastroenterol*, vol. 30, no. 5, pp. 705–718, Sep. 2016.

[7] B. Akpunonu, J. Hummell, J. Akpunonu, and S. Ud Din, "Capsule endoscopy in gastrointestinal disease: Evaluation, diagnosis, and treatment," *Cleve Clin J Med*, vol. 89, no. 4, pp. 200–211, Apr. 2022.

[8] Q. Tang, G. Jin, G. Wang, T. Liu, X. Liu, B. Wang, and H. Cao, "Current sampling methods for gut microbiota: A call for more precise devices," *Front Cell Infect Microbiol*, vol. 10, p. 151, Apr. 2020.

[9] R. Del-Rio-Ruiz, D. R. Romualdo da Silva, H. Suresh, H. Creasey, C. Asci, D. M. dos Santos, A. Sharma, G. Widmer, and S. Sonkusale, "Soft autonomous ingestible device for sampling the small-intestinal microbiome," *Device*, vol. 2, no. 8, p. 100406, 2024.

[10] N. K. Mandsberg, G. Moro, M. Ghavami, S. B. Andersen, E. N. de Visser, M. F. Bertelsen, M. S. Mortensen, T. R. Licht, and A. Boisen, "Ingestible Device for Gastric Fluid Sampling," *Advanced Materials Technologies*, vol. 9, no. 17, pp. 1–14, 2024.

[11] S. Nejati, J. Wang, U. Heredia-Rivera, S. Sedaghat, I. Woodhouse, J. S. Johnson, M. Verma, and R. Rahimi, "Small intestinal sampling capsule for inflammatory bowel disease type detection and management," *Lab on a Chip*, vol. 22, no. 1, pp. 57–70, 2022.

[12] M. Rehan, I. Al-Bahadly, D. G. Thomas, W. Young, L. K. Cheng, and E. Avci, "Smart capsules for sensing and sampling the gut: status, challenges and prospects," *Gut*, vol. 73, no. 1, pp. 186–202, 2023.

[13] H. Rezaei Nejad, B. C. M. Oliveira, A. Sadeqi, A. Dehkharghani, I. Kondova, J. A. M. Langermans, J. S. Guasto, S. Tzipori, G. Widmer, and S. R. Sonkusale, "Ingestible osmotic pill for in vivo sampling of gut microbiomes," *Advanced Intelligent Systems*, vol. 1, no. 5, p. 1900053, 2019.

[14] P. Shokrollahi, Y. P. Lai, S. Rash-Ahmadi, V. Stewart, M. Mohammadigheisar, L.-A. Huber, N. Matsuura, A. E. H. Zavodni, J. Parkinson, and E. Diller, "Blindly controlled magnetically actuated capsule for noninvasive sampling of the gastrointestinal microbiome," *IEEE/ASME Transactions on Mechatronics*, vol. 26, no. 5, pp. 2616–2628, 2021.

[15] T. Lee and E. Diller, "Magnetic Capsule for Stable Collection of Large GI Tract Microbiome Samples," *Proceedings of MARSS 2025 - 8th International Conference on Manipulation, Automation, and Robotics at Small Scales*, pp. 1–7, 2025.

[16] Y. Sun, W. Zhang, J. Gu, L. Xia, Y. Cao, X. Zhu, H. Wen, S. Ouyang, R. Liu, J. Li, Z. Jiang, D. Cheng, Y. Lv, X. Han, W. Qiu, K. Cai, E. Song, Q. Cao, and L. Li, "Magnetically driven capsules with multimodal response and multifunctionality for biomedical applications," *Nature Communications*, vol. 15, no. 1, pp. 1–14, 2024.

[17] S. Nejati, J. Wang, U. Heredia-Rivera, S. Sedaghat, I. Woodhouse, J. S. Johnson, M. Verma, and R. Rahimi, "Small intestinal sampling capsule for inflammatory bowel disease type detection and management," *Lab Chip*, vol. 22, no. 1, pp. 57–70, Dec. 2021.

[18] M. Rehan, I. Al-Bahadly, D. G. Thomas, and E. Avci, "Development of a robotic capsule for in vivo sampling of gut microbiota," *IEEE Robotics and Automation Letters*, vol. 7, no. 4, pp. 9517–9524, 2022.
[19] M. Finocchiaro, C. Giosuè, G. Drago, F. Cibella, A. Menciassi, M. Sprovieri, and G. Ciuti, "Design of a magnetic actuation system for a microbiota-collection ingestible capsule," in *2021 IEEE International Conference on Robotics and Automation (ICRA)*, 2021, pp. 6905–6911.
[20] Q. Cao, R. Deng, Y. Pan, R. Liu, Y. Chen, G. Gong, J. Zou, H. Yang, and D. Han, "Robotic wireless capsule endoscopy: recent advances and upcoming technologies," *Nat Commun*, vol. 15, no. 1, p. 4597, May 2024.
[21] M. Rehan, I. Al-Bahadly, D. G. Thomas, and E. Avci, "Towards gut microbiota sampling using an untethered sampling device," *IEEE Access*, vol. 9, pp. 127 175–127 184, 2021.
[22] C. W. Fountain, J. Jennings, C. K. McKie, P. Oakman, and M. L. Fetterolf, "Viscosity of common seed and vegetable oils," *Journal of Chemical Education*, vol. 74, no. 2, p. 224, Feb 1997.
[23] S. K. Lai, Y.-Y. Wang, D. Wirtz, and J. Hanes, "Micro- and macrorheology of mucus," *Advanced Drug Delivery Reviews*, vol. 61, no. 2, pp. 86–100, 2009.
[24] A. Agcal, S. Ozcira, and N. Bekiroglu, "Wireless power transfer by using magnetically coupled resonators," in *Wireless Power Transfer*, E. Coca, Ed. Rijeka: IntechOpen, 2016, ch. 3.
[25] T. Campi, S. Cruciani, F. Maradei, and M. Feliziani, "A new transmitting coil for powering endoscopic capsules using wireless power transfer," *Electronics*, vol. 12, no. 8, 2023.
[26] H. Z. Dailiana, D. Kotsaki, S. Varitimidis, S. Moka, M. Bakarozi, K. Oikonomou, and N. K. Malizos, "Injection injuries: seemingly minor injuries with major consequences," *Hippokratia*, vol. 12, no. 1, pp. 33–36, Jan. 2008.
[27] J. Liu, H. Sugiyama, T. Nakayama, and S. Miyashita, "Magnetic sensor based topographic localization for automatic dislocation of ingested button battery," in *2020 IEEE International Conference on Robotics and Automation (ICRA)*, 2020, pp. 5488–5494.